Colloids and Surfaces B: Biointerfaces 80 (2010) 94–102

Contents lists available at ScienceDirect

Colloids and Surfaces B: Biointerfaces

journal homepage: www.elsevier.com/locate/colsurfb

Extracellular biosynthesis and transformation of selenium nanoparticles and application in H_2O_2 biosensor

Tingting Wang[a,b], Liangbao Yang[a,*], Buchang Zhang[b], Jinhuai Liu[a,*]

[a] The Key Laboratory of Biomimetic Sensing and Advanced Robot Technology, Anhui Province, Institute of Intelligent Machines, Chinese Academy of Science, Hefei, 230031 Anhui, PR China
[b] School of Life Science, Anhui University, Hefei, Anhui 230039, PR China

ARTICLE INFO

Article history:
Received 27 April 2010
Received in revised form 26 May 2010
Accepted 26 May 2010
Available online 1 June 2010

Keywords:
Se nanoparticles
Transformation
Bacillus subtilis
H_2O_2 biosensor

ABSTRACT

We reported a very simple, reliable, clean, nontoxic and eco-friendly biological method for the synthesis of semiconductor monoclinic Se nanoparticles by the *Bacillus subtilis*. The as-synthesized Se nanoparticles were spherical shaped with diameters ranging from 50 to 400 nm. These spherical monoclinic Se nanoparticles can be transformed into highly anisotropic, one-dimensional (1D) trigonal structure after one day at the room temperature and grown from aqueous solutions. Furthermore, the obtained two kinds of Se nanomaterial crystals with high surface-to-volume ratio, good adhesive ability and biocompatibility have been employed as enhancing and settled materials for H_2O_2 biosensor. The results show that the H_2O_2 biosensor has high sensitivity and affinity for H_2O_2. The detection limit for H_2O_2 was found to be 8×10^{-8} M. Different crystals of Se nanomaterials have no significant difference in electrochemical application.

1. Introduction

Nanomaterials have conspicuous physicochemical properties that remarkably differ from those of bulk materials. So they have attracted a great deal of attention and are potential for wide-ranging applications [1]. The semiconductor nanoparticles have excellent nonlinear properties, saturable absorption, and optical bistability. As an important semiconductor, Se attracts more attention because of its special physical properties, such as the anisotropy of thermoconductivity, superconductivity, catalytic activities to hydration and oxidation reactions, and high piezoelectric, thermoelectric, and nonlinear optical responses [2]. So, Se plays important roles in many applications, such as photocells, photographic exposure meters, and solar cells to semiconductor rectifiers [3]. In addition, Se is one of the key elements for maintaining the health of mammalian animals because it exerts anti-oxidative [4] and pro-oxidative effects [5]. Moreover, several studies indicated that some organic forms of Se could show anticarcinogenic properties against certain types of cancer [6,7].

In the past few years, many methods about the synthesis of Se nanostructures have been developed. For example, Gates et al. have described a soft, solution-phase approach to the large-scale synthesis of uniform nanowires of trigonal selenium (t-Se) [8]. Xie and his co-workers have developed a novel, convenient acidification approach to the preparation of Se nanowires with a typical diameter of 50 nm and a typical length of 5 μm in a polymer buffer system at room temperature [9]. Cao et al. have also developed a simple and convenient physical vapor deposition route for fabricating nanowire networks of t-Se on a solid support by their spontaneously organized growth during the crystallization period [10]. Ma et al. have synthesized single-crystalline nanobelts and nanowires of t-Se in micellar solutions of nonionic surfactants [11]. Jeong's group has successfully observed the transformation process of a-Se into t-Se nanowires on solid substrates [12]. Chen et al. have used L-cysteine as both the reducing agent and soft template to control the synthesis of Se nano-spheres [13]. Our team has reported the formation of Se microwire networks by hydrothermal treatment in tungstosilicic acid solution [14]. We also describe the formation of α-Se/protein composites using *Capsicum annuum L* extract at room temperature [15].

To our knowledge, most of these syntheses of Se 1D nanostructures are physical and chemical methods, they are characterized by elevated temperatures, long growth times, high pressures, low yields, and are also environmentally hazardous [15]. However, how to develop a reproducible, eco-friendly and simple method to synthesize stable Se nanoparticles with good biological activity is still a challenge. There is an interesting and exciting biogenic synthesis to prepare various nanomaterials, the synthesis of nanomaterials by biological systems occurs at close to ambient temperatures and pressures, and at neutral pH [16]. This method is a clean, nontoxic and environmentally friendly procedure. Besides, the synthesized materials are biologically compatible [17]. In addition, biological

* Corresponding authors. Tel.: +86 551 5591142; fax: +86 551 5592420.
E-mail addresses: lbyang@iim.ac.cn (L. Yang), jhliu@iim.ac.cn (J. Liu).

0927-7765/$ – see front matter © 2010 Elsevier B.V. All rights reserved.
doi:10.1016/j.colsurfb.2010.05.041

synthesis can present extra advantages over chemical methods such as higher productivity and lower cost [18]. Attempts have been made to synthesize nanomaterials from such microorganisms as bacteria [19], fungi [17] and yeast [20]. However, a bacterial system is preferred mainly due to reduced time of reaction, ease in handling, and easy genetic manipulation.

H_2O_2 is harmful to biological systems and appears to be involved in the neuropathology of central nervous system diseases [21]. H_2O_2 also has an indirect impact on the acid rain procedure that is harmful to the atmosphere [22]. In addition, H_2O_2 is an essential mediator in food, pharmaceutical, clinical, industrial and environmental analyses. So the reliable, accurate and rapid detection of H_2O_2 is of practical importance [23]. Several groups developed some biosensors based on the electrocatalysis of immobilized enzymes to reduction H_2O_2. In Wang's study, a chemiluminescent (CL) H_2O_2 sensor based on horseradish peroxidase (HRP) immobilized by sol–gel method was proposed. The sensor provided a long lifetime and showed a linear response toward H_2O_2, with a detection limit of 8 μM [24]. Dong's group developed a novel method to construct a third-generation HRP biosensor by self-assembling AuNPs into three-dimensional sol–gel network. The detection limit of the biosensor could attain 2.0 μM, and the linear range was between 5.0 μM and 10.0 mM [25]. Guo's group completed direct electrochemistry of cytochrome *c* on a novel electrochemical interface constructed by self-assembling AuNPs onto a three-dimensional silica gel network, this biosensor exhibited a fast amperometric response (5 s), a good wide linear range of concentrations from 5.0×10^{-6} to 1.4×10^{-3} M, and a low detection limit of 4.01×10^{-7} M [26]. In this paper, we deposited Se nanomaterials onto the surface of GC electrodes, and then HRP was dropped on the surface of the above-modified electrode. This modificatory biosensor showed good analytical performance, lower detection limit as compared with above researches.

Herein we report a facile, economical and green biological route for the synthesis of monoclinic Se (m-Se) nano-spheres with *Bacillus subtilis*. It is easy to handle and can be manipulated genetically without much difficulty, and it is also harmless to humans. In our work, although the exact mechanism leading to reduction of SeO_3^{2-} ions to elemental selenium form is yet to be elucidated, it is possible that certain biochemical reducing agents are excreted by the *B. subtilis* only in response to precursors 'stress' [20]. The proteins excrete from the bacteria which could be used as reductants and scaffolds for the synthesis of m-Se, and can even participate in the formation of m-Se/protein composites. These spherical monoclinic Se nanoparticles can be transformed into trigonal structure after keeping for one day at room temperature. It is found that the as-prepared two kinds of nano-Se nanomaterials with high surface-to-volume ratio, good adhesive ability and biocompatibility, are expected to exhibit high electrocatalytic activities to detect H_2O_2. The as-proposed sensor showed good analytical performance and low detection limit.

2. Experimental

2.1. Materials

B. subtilis seed was gotten from Anhui University School of Life Science. Sodium selenite was of A.R. grade and was obtained from Shanghai Reagent Co. Horseradish peroxidase (HRP) was obtained from Shanghai Reagent Co. LB medium: 1.0 g tryptone, 0.5 g yeast extract, 1.0 g NaCl, in 100 ml H_2O; pH adjusted to 7.0 with 10 μl NaOH. Enrichment (EM) medium: 0.1 g $NaNO_3$, 1 g NaCl, 0.02 g NH_4Cl, 0.54 g K_2HPO_4, 0.6 g tryptone, 0.2 g beef extract, 0.1 g yeast extract, 0.6 g glucose, in 200 ml H_2O. A 0.2 M phosphate buffer solution (PBS) (pH 7.0) consisting of NaH_2PO_4 and Na_2HPO_4 was employed as the supporting electrolyte. The water used in this experiment was double distilled water. All the reagents were used without further purification.

2.2. Bacterial growth conditions

For the growth of the bacterium, seed culture was inoculated in 100 ml of Luria-Bertani (LB) medium in 500 ml of Erlenmeyer flask. The flask was then incubated at 35 °C on a rotary shaker (170 rpm). After 12 h of bacterial growth, the *B. subtilis* was collected for further experiments.

2.3. Synthesis of Se/protein composites using B. subtilis

0.069 g sodium selenite (4 mM) and 1 ml activated *B. subtilis* were added into 100 ml EM medium, this reaction solution was allowed to react completely for 48 h at 35 °C on a rotary shaker (170 rpm). With the reaction, the color of solution changed from clear light-yellow to red. The red color of solution indicates the presence of Se nanoparticles in solution. The red Se nanoparticles were harvested by centrifugation at 10,000 rpm for 6 min (the Se nanoparticles were harvested by separating bacterial biomass by centrifugation at 3000 rpm if it was necessary), then washed with double distilled water and absolute ethanol several times and analyzed by different characterization techniques. The harvested samples were deposited at room temperature. In our experiments, it is found that different concentrations of sodium selenite did not affect the morphology of the final products.

In the control experiment, the activated *B. subtilis* were heated at 100 °C for 1 h, and then added to 100 ml EM medium with 0.069 g sodium selenite (4 mM), the same reaction was allowed to react completely for 48 h at 35 °C on a rotary shaker (170 rpm), but the color of the reaction solution did not change. Another control experiment was performed wherein the activated *B. subtilis* was filtered, and the filtrate was reacted with sodium selenite (4 mM). It was observed that the color of solution changed to red similar to that shown in the typical experiment, the details are complemented by the supporting information.

2.4. The preparation of HRP biosensor

The glassy carbon (GC, 3 mm diameter) electrode was polished before each experiment with alumina powder, rinsed thoroughly with doubly distilled water between each polishing step, then washed successively with 1:1 nitric acid, acetone and doubly distilled water in ultrasonic bath and dried in air. The modified electrode was prepared by dripping 10 μl Se nanoparticles (m-Se and t-Se, respectively) on GC surface, and dried under an infrared lamp. Then, 10 μl HRP (pH 7.8, 2 mg ml^{-1}) was dropped on the surface of above-modified electrode. Electrochemical experiments (H_2O_2 sensing) were performed under the N_2 condition (the N_2 purity is 99.99%). Cyclic voltammetry scans were performed in a 0.1 M PBS buffer solution (pH 7.4) and operated from −0.6 to 0.4 V (vs. Ag/AgCl) with scan rate 0.05 V s^{-1}. Replicate measurements were performed by renewing the surface and repeating the above assay preparation procedure. The modified electrode was stored at 4 °C in a refrigerator when not used.

2.5. Characterization of selenium nanoparticles

The size and morphology of the synthesized selenium nanomaterials were analyzed by using a Quanta 200 (FEG Co. Ltd.) field emission scanning electron microscope at an accelerating voltage of 5.0 kV. All TEM images were carried out on a JEM model 100SX electron microscope instrument (Japan Electron Co.) operated at an accelerating voltage at 200 kV. XPS measurements of the samples

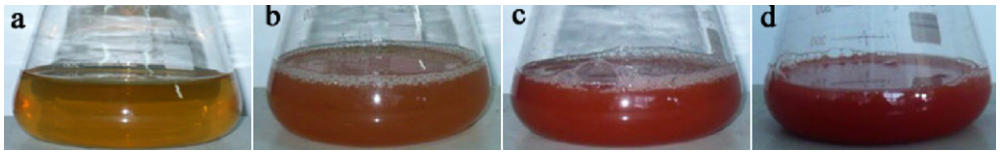

Fig. 1. The time-dependent color changes of the reaction solution, (a), (b), (c) and (d) represent 12, 24, 36 and 48 h, respectively (For interpretation of the references to color in this figure legend, the reader is referred to the web version of the article.).

were carried out on a VG ESCALAB MKII instrument at a pressure greater than 10^{-6} Pa. The general scan and Se_{3d}, N_{1s}, O_{1s} and C_{1s} core level spectra were recorded with un-monochromatized Mg Kα radiation (photon energy = 1253.6 eV). The core level binding energies (BEs) were aligned with respect to the C_{1s} binding energy (BE) of 285 eV. XRD analysis of the samples was carried out on a MAP18A-H F instrument (Japan MAC Science Co.). The optical characteristics of the synthesized m-Se were measured using UV–vis spectroscopy measurements, the samples were carried out on a TU-1901 model UV–vis double beam spectrophotometer (Beijing Purkinje General Instrument Co., Ltd., China) operated at a resolution of 2 nm. Raman spectra of the selenium nanomaterials were recorded on a confocal lasermicro-Raman spectrometer (JY Labram-HR), using 24 mW excitation at 532 nm.

3. Results and discussion

After exposing activated *B. subtilis* to sodium selenite and incubating for 48 h in the EM medium at 35 °C, and the reaction solution displayed a time-dependent color change, as shown in Fig. 1. At the beginning of reaction, the solution was clear light-yellow, and it became light red after 24 h of reaction; the light red changed into red gradually at 48 h, and then the red color did not change obviously with increasing reaction time. The appearance of the red color indicated the occurrence of the reaction and the formation of Se solution. m-Se was red and the glass-transition temperature of Se was around 31 °C [27], indicating a m-Se structure of the as-synthesized products. The characteristic red color of the reaction solution was due to excitation of the surface plasmon vibrations of the m-Se particles and provided a convenient spectroscopic signature of their formation [28]. In the control experiment, when the activated *B. subtilis* was heated at 100 °C for 1 h, the other reaction conditions remaining the same, the color of the reaction solution did not change, indicating that sodium selenite need not be reduced. (The data was not shown) The reason was that high temperature made the proteins lose action and they did not function in the reaction.

The morphology and dimension of m-Se collected from the reaction solution were examined by FESEM. Fig. 2 showed that the product obtained from the reaction solution after 12, 24, 36 and 48 h of reaction. We could see that the synthesized Se nanoparticles were spherical shapes and become more and larger with the times prolonging. Fig. 2(b) showed that there are plenty of particles with a size of several nanometers among the bacteria. The larger particles could grow from the smaller ones. After aging for 24 h, the particles had already grown to about 50–150 nm, and there was evidence of the final spherical structure. After aging for 48 h, a very large percentage of the nanoparticles had grown with the diameter from 50 to 400 nm (Fig. 2(d)). From this image, it appeared that the growth of Se crystallites proceeded from within the precursor small particles and led to their assembly on the surface of the precursor small particles. The particles had evolved considerably in size and shape, and exhibited a distinct and highly regular morphology. The overall morphology of the particles underwent a clear resemblance to the final spherical morphology. This transformation process with small nanoparticles as precursors was a typical Ostwald ripening

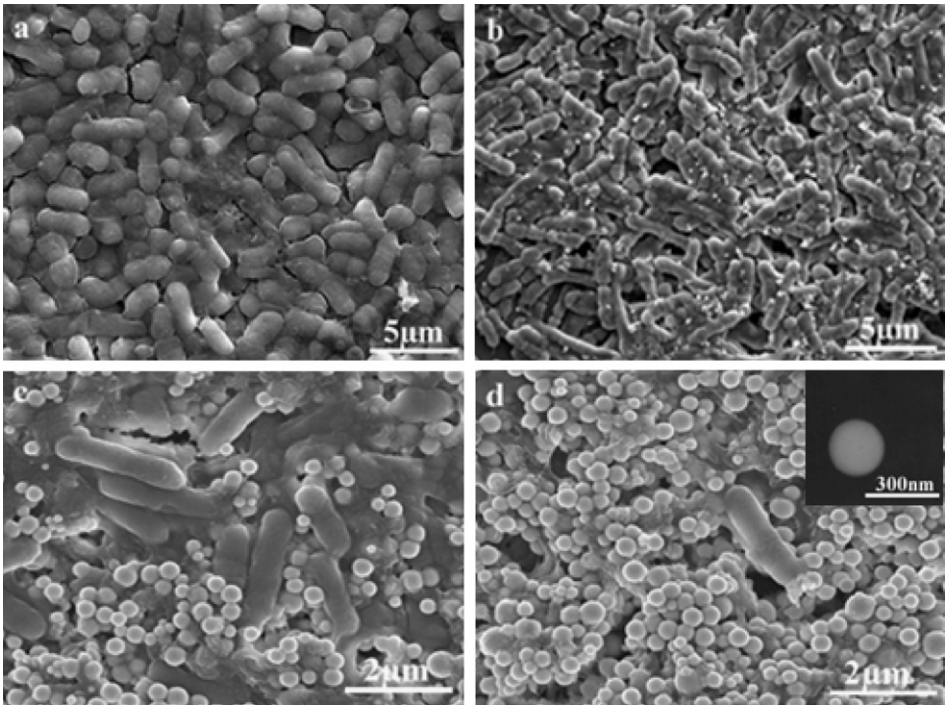

Fig. 2. FESEM images of the prepared m-Se nano-sphere at different reaction times, (a), (b), (c) and (d) represent 12, 24, 36 and 48 h, respectively. The inset in (d) is the TEM micrograph of the sample in 48 h.

process. The inserted TEM image of the sample in Fig. 2(d) provided further evidence that the as-synthesized samples had a spherical morphology with smooth surface. Usually, m-Se tended to form a spherical morphology with a smooth surface [29].

To further investigate for the purities and compositions of the products. X-ray photoelectron spectra (XPS) were recorded. The products were harvested from the reaction solution by a series of disposals. The general scan spectrum showed the presence of strong C_{1s}, O_{1s}, N_{1s} and Se_{3d} core levels shown in Fig. 3(a), the XPS spectrum of the Se_{3d} core levels was not nakedness, in other words, the intensity of the emission peak was very weak, it may be attributed to the fact that the Se nanoparticles were easily coated by some proteins excreted from *B. subtilis*. The similar phenomena also appeared in our another latest report about a very simple and novel one-step method to synthesize silver–core–gold–shell by in situ sunlight-reduction in $AgNO_3$ solution and $NaAuCl_4$ solution in the presence of DNA [30]. Fig. 3(b) showed the XPS spectrum of the Se_{3d} core levels. The binding energy (BE) at 55.74 eV was the characteristic peak for elemental Se [31]. The N_{1s} shown in Fig. 3(c) could be centered at 402.3 eV, which matched closely with N_{1s} BE in amide bonds [32]. The O_{1s} core level shown in Fig. 3(d) was broad and centered at 533.5 eV, and was assigned to the carboxylate groups [33]. The C_{1s} core level shown in Fig. 3(e) could be decomposed into three chemically distinct components present in protein molecules. Three curves corresponded to the chemically distinct C_{1s} core levels originating from the hydrocarbon chains, a-carbon and –COOH groups present in the protein–Se composite with BEs of 284.7, 286.3 and 288 eV, respectively [34]. The presence of C, N, O was probably due to the presence of contaminating proteins and other biopolymers in the sample [20], which was in agreement with the results of XRD (see below). Thus, it can be concluded from the XPS measurements that not only was the element Se synthesized, but also the small sized m-Se nanoparticles were capped by proteins excreted from *B. subtilis*, and the protein played an important role for the formation of m-Se.

As shown in Fig. 4, the protein absorption peak appeared at 280 nm concomitantly. Compared to curve a in Fig. 4, the intensity of the protein absorption peak in curve b and c was decreased. It could be attributable to the reaction between the SeO_3^{2-} ions and the proteins excreted from *B. subtilis*. It suggested that the protein played important roles in the reduction of SeO_3^{2-} ions to Se^0 and the formation of composites. Quite interestingly, the solution was stable with no evidence of flocculation of the particles even a month after reaction at 4 °C. We believe that the long-term stability of the

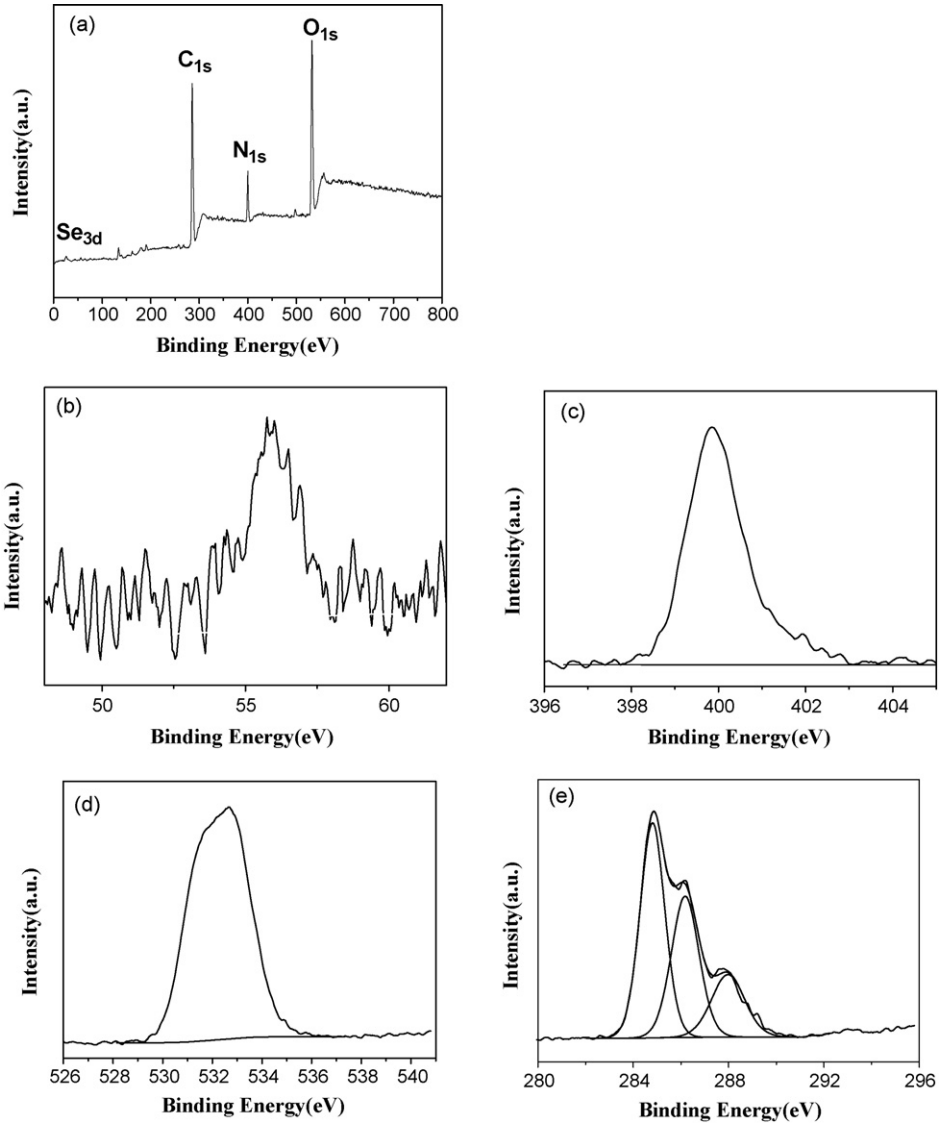

Fig. 3. (a) The general XPS of the resultant m-Se nanosphere. (b) Spectra of the Se_{3d} core level, (c) N_{1s} core level, (d) O_{1s} core level and (e) C_{1s} core level.

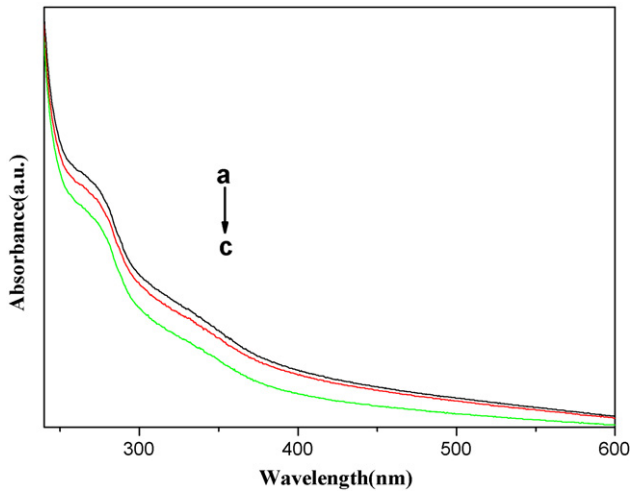

Fig. 4. Time dependence of the UV–vis spectrum of the reaction solution, (a) 12 h, (b) 24 h and (c) 48 h (with a spectrophotometer quartz cuvette:1 cm × 1 cm).

nanoparticle solution is due to the presence of the proteins in the nanoparticle solution that bind to the surface of the nanoparticles and prevent aggregation.

When the harvested samples were deposited at the room temperature, the color of solution changed gradually to black after one day, indicating the spontaneous transformation of Se from monoclinic to trigonal structure. We also followed the nucleation and growth steps of the transformation process (taken at various stages of aging time) with FESEM. Fig. 5 showed the SEM and TEM images of three samples prepared at different times. Fig. 5(a) clearly revealed the formation of colloids as uniform nano-spheres. When this solution was aged at room temperature for 12 h, there was mixture of m-Se nanoparticles and t-Se nanowires(Fig. 5(b)). The t-Se nanowires were actinomorphic. The colloids would slowly dissolve into the solution phase due to the higher free energy of m-Se as compared to t-Se. The Se dissolved from m-Se colloids could be subsequently deposited on the surfaces of t-Se nanocrystallites acted as seeds and then grew into uniform single-crystalline nanowires (Fig. 5(c)). On the basis of the structure, we believe that the formation of t-Se nanowire is based on the Ostwald ripening process and the oriented attachment mechanism. Such spontaneous self-aggregation and crystallization induced by the crystallized seeds is very similar to our earlier study [14]. The high-magnification SEM image shown in Fig. 5(d) revealed that Se nanowires had a mean diameter of 100 nm and a standard deviation of 10 nm. Some of the nanowires aggregated into bundles in the solution or during the preparation of SEM sample. This may explain why some of the nanowires look wider than the others. Fig. 5(e) and (f) showed the TEM image and the electron diffraction pattern of an individual nanowire prepared from the same reaction solution as shown in (d), the TEM image clearly revealed that the corresponding diameter for the single nanowire was approximately 100 nm,

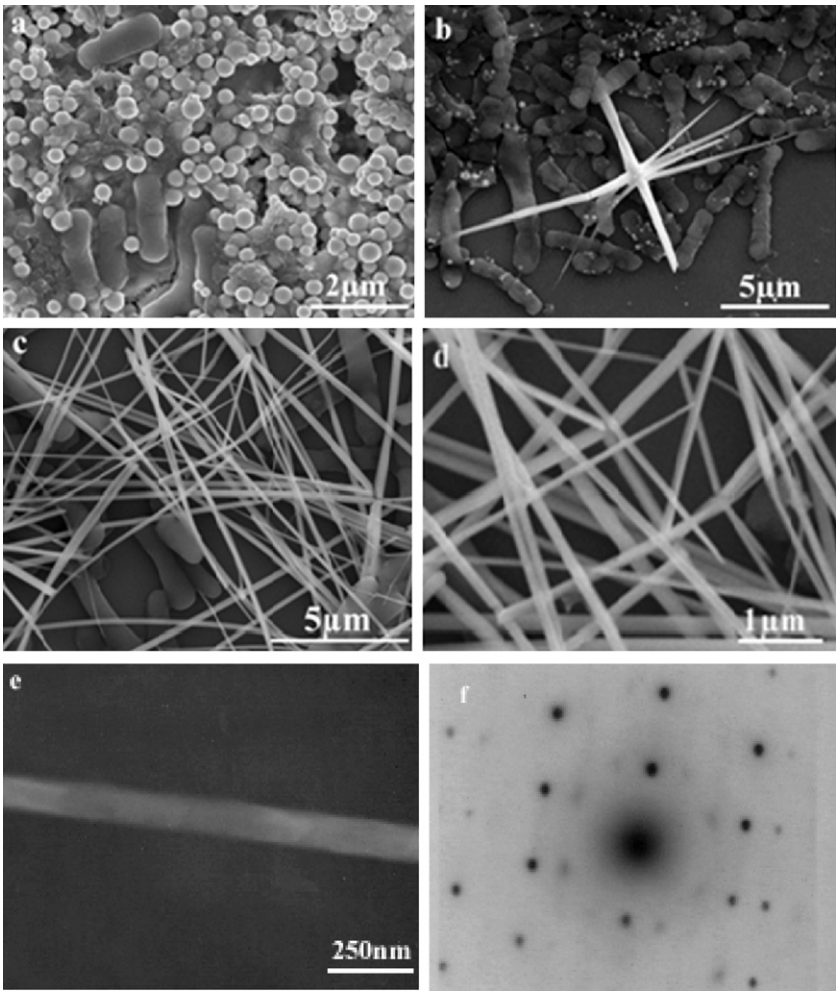

Fig. 5. FESEM and TEM images of the transformation processes from m-Se nano-sphere to t-Se nanowires. (a) The sample was harvested at the room temperature for 0 h, (b) 12 h, (c) 24 h and (d) the high magnification of (c), (e) and (f) the TEM image and the electron diffraction pattern of an individual Se nanowire.

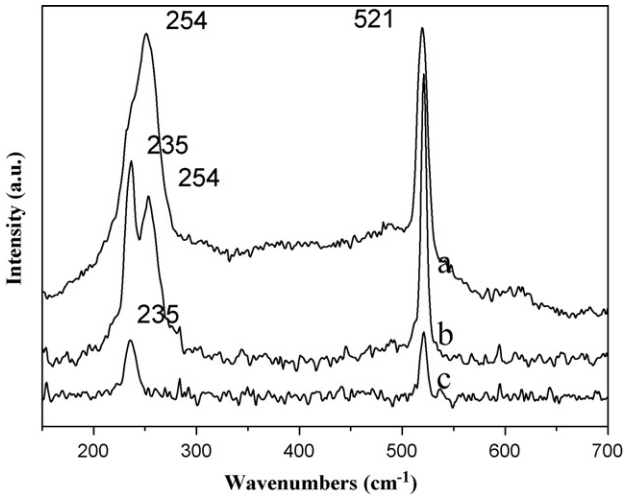

Fig. 6. Raman scattering spectra of the Se species trapped at different stages: (a) the sample is the same of Fig. 5a, (b) the sample is the same of Fig. 5b and (c) the sample is the same of Fig. 5c.

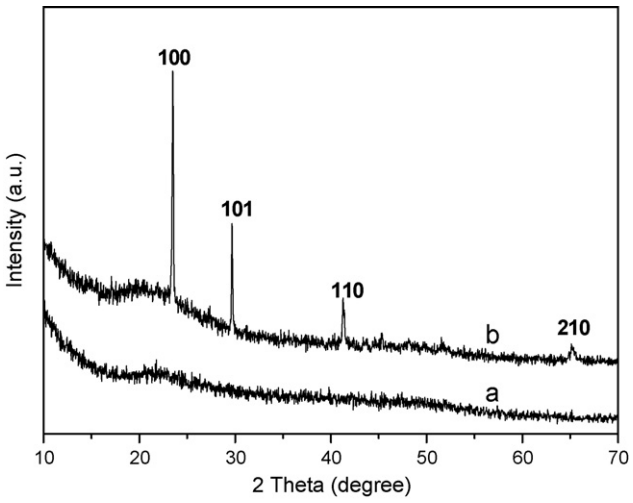

Fig. 7. XRD patterns recorded from drop-coated films on Si (1 1 1) substrates of Se synthesized from different stage. (a) Sample synthesized for 48 h and (b) the sample was harvested at the room temperature for 24 h.

the electron diffraction pattern indicated that the nanowires are single-crystalline. The spots in Fig. 5(f) correspond to the (1 0 0), (1 0 1), (0 0 1), (0 0 3) diffractions from t-Se. The occurrence of the (0 0 1) diffraction may be attributed to the double diffraction of the incident electron in the crystal [9]. These SEM and TEM images indicate the uniformity in lateral dimensions, the straightness along the longitudinal axes, the level of perfection, and the copiousness in quantity that we could routinely achieve for this synthetic system.

The Raman scattering spectrum taken for the as-synthesized Se at different stages was depicted in Fig. 6. The results were in good agreement with the X-ray diffraction data. The distinctive signature of t-Se and m-Se are located at 235 and 256 cm^{-1}, respectively [35]. The curve a in Fig. 6 showed the characteristic m-Se peak centered at 254 cm^{-1}. The curve b in Fig. 6 showed the intermediate state of transformation processes and had both the characteristic peaks of m-Se and t-Se. The results of this study were all very similar to the Ref. [36]. As shown in curve c of Fig. 6, the peak centered at 235 cm^{-1}, which can be assigned to the vibration of the t-Se helical chain. It may be necessary to note that the asymmetric Raman band for Se nanomaterials is broadened. The reason can be attributed mainly to a size effect of the nanomaterials. Besides the characteristic m-Se/t-Se peak, another resonance peak around 521 cm^{-1} was found, which was attributed to the silicon underlay.

The composition and phase of the resultant samples were examined by XRD. Curve a in Fig. 7 showed the XRD pattern of the sample. We presumed precipitation of Se was m-Se, which was in agreement with the results of Raman. There were no clearly sharp Bragg reflections, it may be attributed to the fact that the synthesized Se could be coated by some proteins excreted from the *B. subtilis*, which can be demonstrated by the results of XPS (see above). The background was most likely caused by not enough material for diffraction analysis. Curve b in Fig. 7 showed the XRD pattern of the transformation product of Se nanowires. All the peaks could be in accord with the characteristic peaks of t-Se. All of the strong and sharp reflection peaks can be readily indexed to a single phase of trigonal-structured Se t-Se, space group *P*3121 (152) containing infinite, helical chains of Se atoms packed parallel to each other along the *c*-axis, with cell parameters $a = 0.4367$ nm and $c = 0.4959$ nm. These values agree with the values reported in the literature [10].

Based on the results presented above, we suppose the following model for the reduction of SeO_3^{2-} ions and the transformation of Se from monoclinic nano-spheres to trigonal nanowires. A schematic representation of the formation process of m-Se/protein composites and then t-Se is shown in Fig. 8. The SeO_3^{2-} ions are firstly trapped on the surface of the proteins excreted from the bacteria via electrostatic interaction between SeO_3^{2-} ions and positively charged groups in the protein/enzymes. Then, SeO_3^{2-} ions are reduced by the protein, leading to the formation of Se nuclei (see step 1), which subsequently grew by further reduction of SeO_3^{2-} ions and accumulation of the newly formed Se atoms onto these nuclei. The growth of Se nanoparticles involves an Ostwald ripening mechanism [8]. The larger particles will grow at the expense of small ones according to the well-known Gibbs–Thomson law [37]. Step 1 and 2 are the nucleation and growth steps. The formation of tiny crystalline nuclei in a supersaturated medium occurs at first and is then followed by crystal growth. The flexible linkage of proteins and large numbers of biomolecules in the reaction solutions may lead to the disordered growth of Se (step 3) [15]. The glass-transition temperature is around 31 °C. So, m-Se is formed. Then, these m-Se nanoparticles aggregate into larger spheres in solution. In fact, primary nanoparticles and larger particles of different sizes undergo restructuring or rearranging into a more compact/dense spherical nanoparticle texture, as shown in step 4. Protein keeps the primary nanoparticles and then the larger particles slightly apart, and may provide them with a moderate degree of mobility to regulate their position in the aggregate, which is typically thought to occur in the process of oriented attachment of biomineralization [38]. m-Se is unstable due to its higher free energy relative to that of t-Se and can spontaneously dissolve into the solution to provide Se atoms. The small amount of Se dissolved in the solution precipitated out as single-crystalline nanoparticles of t-Se [39]. The t-Se acts as seed. The Se atoms are transferred to the surface of t-Se seeds. Because the crystal structure of t-Se is composed of a hexagonal array of Se_8 helical chains, the deposition of Se atoms on the seeds is confined to the *c*-axis, leading to the formation of uniform, single-crystal nanowires made of t-Se [40]. At the same time, we thought that proteins played an important role in forming t-Se nanowires in our experiments. In fact, the proteins excreted from the bacteria act as template which quickens transformation of Se from monoclinic nano-sphere to trigonal nanowires. In the former study [36], it usually took 10–20 days to completely convert all the Se colloids into t-Se nanowires at room temperature. In this study, the process only needs one day. As template, proteins not only prohibit the further growth of m-Se, but also form the m-Se/protein composites, and then accelerate the formation of t-Se nanowires

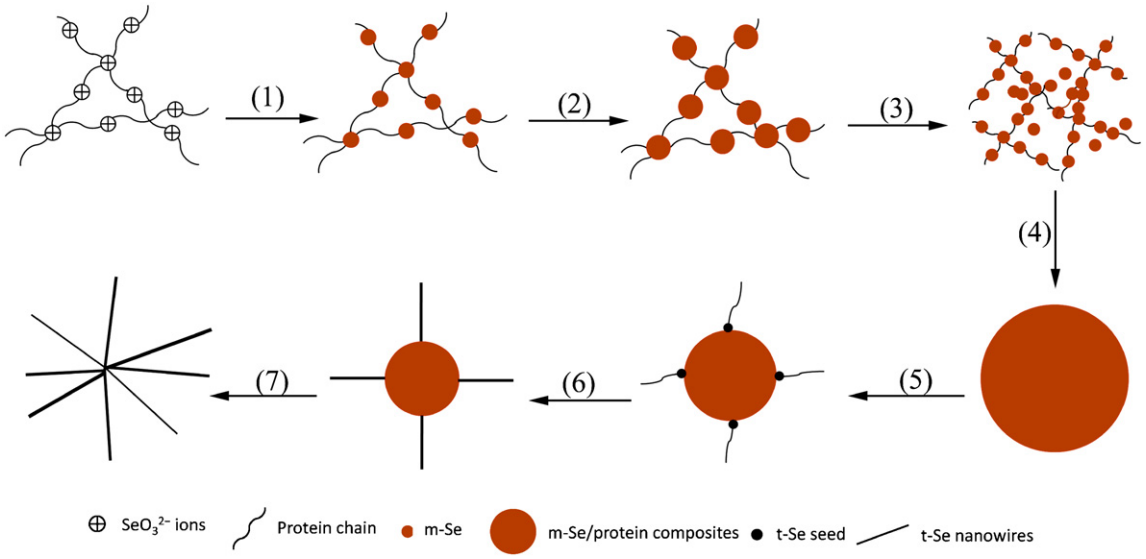

Fig. 8. Schematic illustration of the formation process of m-Se/protein composites and a plausible mechanism for the formation of t-Se nanowires: (1) Reduction of selenious acid with the proteins excreted from the *B. subtilis*; (2) grow by further reduction of SeO_3^{2-} ions and accumulation of the newly formed Se atoms onto these nuclei; (3)and (4) numerous small nanoparticles tend to aggregate into a larger sphere in assembly solution. (5) These spherical colloids split into irregular colloids including protein chains and t-Se seeds, (6) t-Se nanowires continue to grow from the seeds accompanied by the dissolution of m-Se colloidal particles. (7) Formation of actinomorphic nanowires at the complete expense of m-Se colloids.

(see step 4–6). On the other hand, we think that the growth mode for nanowires in this work is similar to the seed-mediated growth mechanism [14]. The so-called wire-directed self-aggregation process in our case is the directional aggregation of the tiny spherelike particles on the backbone of the rods. At last, the actinomorphic nanowires are formed (see step 7).

The as-obtained two kinds of Se nanomaterial crystals with good adhesive ability and biocompatibility can be employed as enhancing and settled materials for HRP biosensor. The Se nanomaterials modified GC electrode was used to study the electrocatalytic activity towards H_2O_2. To verify this statement, we deposited Se nanomaterials onto the surface of GC electrodes, and then HRP was dropped on the surface of the above-modified electrode. It can be seen that the peak currents associated with oxide formation/reduction events provided by the HRP-Se/GC electrode (line b, Fig. 9) are much larger than that of HRP-GC electrode (line a, Fig. 9) (left figure and right figure represent m-Se and t-Se, respectively). The HRP contains heme as a prosthetic group, which is also the protein active site with the resting state of the heme-iron: Fe(II). In addition, it can catalyze the H_2O_2 dependent one-electron oxidation of a great variety of substrates [41]. However, it is difficult for the electron transfer between HRP and electrode to occur [42], but the Se nanomaterials has conductivity, and provides a good micro-environment for electron transport of HRP.

Fig. 10 shows the CVs of assembling Se nanomaterials modified electrode in the absence and presence of H_2O_2 with different concentrations (left figure and right figure represent m-Se and t-Se, respectively). With the increasing concentration of H_2O_2 (curves a–e: $0, 8\times10^{-8}, 8\times10^{-7}, 8\times10^{-6}, 8\times10^{-5}$ M), the H_2O_2 reduction current gradually increases, indicating that the Se nanomaterials modified electrode exhibited good electrocatalytic activity towards H_2O_2. The excellent performance of the electrode is ascribed to the good catalytic activity of the Se nanomaterials and ensemble behavior of the nanoparticle-modified electrode. The presence of nanomaterials on the electrode surface facilitates the electron transfer [43]. In general, the electroanalytical detection limit at a nanoelectrode ensemble can be much lower than that at an analogous macrosized electrode because the ratio between the faradaic and capacitive currents is higher [26]. And our modificatory biosensor shows lower detection limit (8×10^{-8} M) as compared with some reports [24–26]. The electrocatalytic response on the nanomaterials modified electrode is very stable; the peak potential and

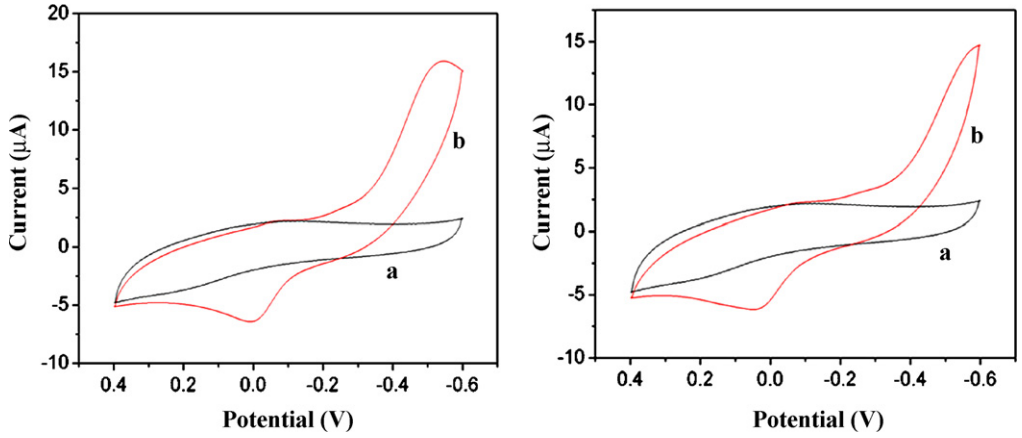

Fig. 9. CVs of HRP-GC (a) and HRP-Se/GC (b) electrodes in 0.2 mM PBS (pH 7.0). (Left and right represent m-Se and t-Se, respectively).

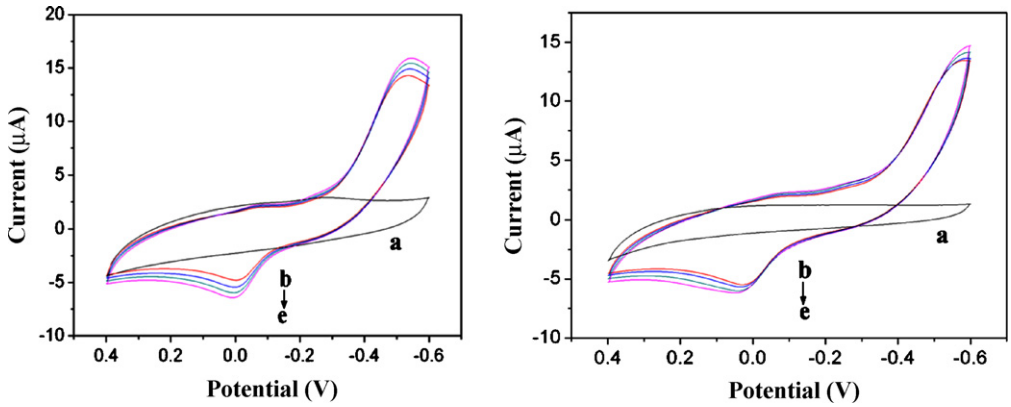

Fig. 10. CVs of assembling Se nanomaterials modified electrode in N_2-saturated PBS (pH 7.0) in the absence and presence of H_2O_2 with different concentrations (curves a–e: 0, 8×10^{-8}, 8×10^{-7}, 8×10^{-6}, 8×10^{-5} M). Scan rate: 50 mV s^{-1}. (Left and right represent m-Se and t-Se, respectively).

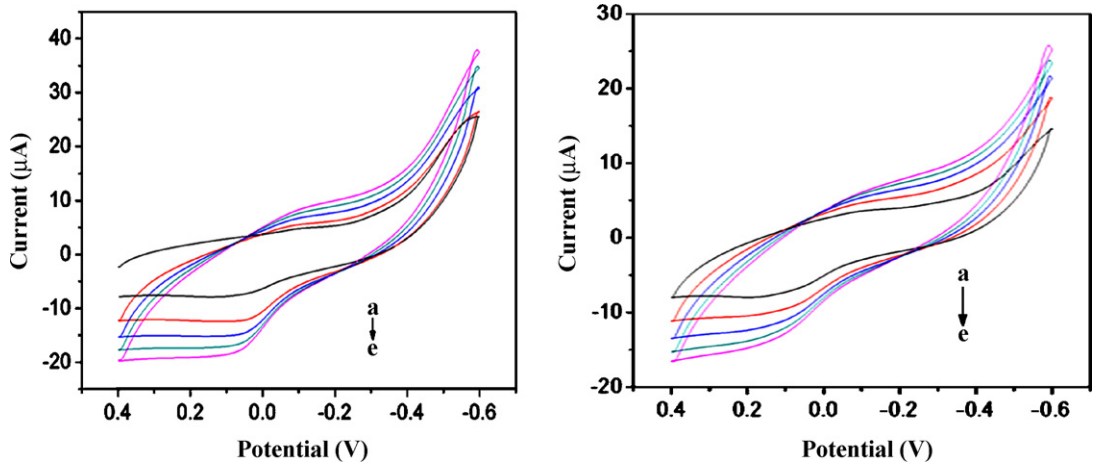

Fig. 11. CVs of Se nanomaterials modified electrode in N_2-saturated PBS (pH 7.0) in the presence of 0.8 mM H_2O_2 at different scan rates (curves a–e: 50, 100, 200, 300, 400, 500 mV s^{-1}). (Left and right represent m-Se and t-Se, respectively).

peak current do not change upon repeated sweeps. The m-Se-modified electrode shows a lower potential than the t-Se-modified electrode, but has no other significant differences in electrochemical application, the reasons and the details of this mechanism are still being researched.

Furthermore, the electrocatalytic behavior of the Se nanomaterials modified electrode to H_2O_2 was further studied with the change of scan rate. As shown in Fig. 11 (left figure and right figure represent m-Se and t-Se, respectively), the CVs at different scan rates are typical of a quasi-reversible redox process. Increasing with scan rate from 0.05 to 0.5 V s^{-1}, the cathodic peak current increases, indicating it was a diffusion-controlled process [44].

At present, one challenge in the nanotechnology area is the fabrication and interconnection of enzymes with nanostructured materials and various approaches have been explored toward the conjugation [45,46]. Classical methods for immobilizing enzymes are physical adsorption, entrapment and covalent cross-linking, which have shortcomings such as the leakage and partial denaturation of the enzyme. Compared with traditional macroscale materials, nanostructured materials have large surface-to-volume ratios, which enable nanostructured materials to have potential to serve as superior enzyme supports [47]. In this study, the obtained Se nanomaterials with good adhesive ability and biocompatibility are employed as enhancing and settled materials for H_2O_2 biosensor. The results show that the H_2O_2 biosensor has high sensitivity and affinity for H_2O_2. All these features, along with electrocatalytic characteristics of the reduction of H_2O_2, indicate that HRP immobilized on the Se nanomaterials keeps intrinsic and good electrocatalytic activities towards its substrates. The biocompatibility of Se nanoparticles enables the nanomaterial to become a good biosensing platform for realizing direct electrochemistry and electrocatalysis of heme-containing proteins/enzymes [48].

4. Conclusions

In summary, m-Se nanoparticles with spherical shapes can be synthesized in a large scale by reaction of a mixture of *B. subtilis* and sodium selenite under ambient temperatures, ambient pressures, and at neutral pH. Reduction of the SeO_3^{2-} ions and stabilization of m-Se were believed to occur by the participation of protein and other biomolecules excreted from *B. subtilis*. The exact reduction mechanism is also being investigated. This attractive strategy provides an economical and facile route for the synthesis of a wide range of functional biocomposites consisting of biomolecules and m-Se particles. The as-prepared two kinds of nano-Se crystals have been used as enhancing and settled materials for building HRP biosensor. The obtained sensor exhibits good electrocatalytic activity towards the reduction of H_2O_2 due to the good adhesive ability and biocompatibility of Se nanomaterials. The detection limit for H_2O_2 was found to be 8×10^{-8} M. Most importantly, the Se nanomaterials modified electrode will probably be promising for a wide range of applications related to the detection of H_2O_2 in food, pharmaceutical, clinical, industrial and environmental analyses.

The proteins excreted from the bacteria act as template which quickens transformation of Se from monoclinic nano-sphere to trigonal nanowires at room temperature. We believe the synthetic strategy described here can be scaled up for the high-volume production of t-Se nanowires that can subsequently serve as the physical or chemical templates to generate 1D nanostructures of various kinds of functional materials. The synthetic strategy itself may also be extendable to other systems containing chain-like building blocks [36].

Acknowledgements

The financial support of this work by the National Science Foundation of China (project no. 60574095), National Basic Research Program of China (2007CB936603 and 2009CB939902), China Postdoctoral Science Foundation funded project (20070420739) and Hi-tech Research and Development Program of China (863 Program) (2009AA03Z330) are gratefully acknowledged.

Appendix A. Supplementary data

Supplementary data associated with this article can be found, in the online version, at doi:10.1016/j.colsurfb.2010.05.041.

References

[1] L. Manna, E.C. Scher, A.P. Alivisatos, J. Am. Chem. Soc. 122 (2000) 12700–12706.
[2] L.I. Berger, Semiconductor Materials, CRC Press, Boca Raton, FL, 1997.
[3] V.V. Poborchii, A.V. Kolobov, K. Tanaka, Appl. Phys. Lett. 74 (1999) 215–217.
[4] Y.P. Bao, G. Williamson, Prog. Nat. Sci. 10 (2000) 321–330.
[5] H.M. Shen, C.F. Yang, W.X. Ding, J. Liu, C.N. Ong, Free Radic. Biol. Med. 30 (2001) 9–21.
[6] R.D. Ellis, E.D. Salt, Curr. Opin. Plant Biol. 6 (2003) 273–279.
[7] H. Tapiero, D.M. Townsend, K.D. Tew, Biomed. Pharmacother. 57 (2003) 134–144.
[8] B. Gates, B. Mayers, B. Cattle, Y.N. Xia, Adv. Funct. Mater. 12 (2002) 219–227.
[9] X. Zhang, Y. Xie, F. Xu, X.H. Liu, S.Y. Zhang, X.B. Tian, Solid State Sci. 5 (2003) 525–527.
[10] X.B. Cao, Y. Xie, L.Y. Li, Adv. Mater. 15 (2003) 1914–1917.
[11] Y. Ma, L.M. Qi, W. Shen, J.M. Ma, Langmuir 21 (2005) 6161–6164.
[12] S. Ko, G.D. Moon, U. Jeong, Nanotechnology 19 (2008) 345601–345606.
[13] Z.X. Chen, Y.H. Shen, A.J. Xie, J.M. Zhu, Z.F. Wu, F.Z. Huang, Cryst. Growth Des. 9 (2009) 1327–1333.
[14] L.B. Yang, Y.H. Shen, A.J. Xie, J.J. Liang, Eur. J. Inorg. Chem. (2007) 4438–4444.
[15] S.K. Li, Y.H. Shen, A.J. Xie, X.Y. Yu, X.Z. Zhang, L.B. Yang, C.H. Li, Nanotechnology 18 (2007) 405101–405109.
[16] A. Bharde, D. Rautaray, V. Bansal, A. Ahmad, I. Sarkar, S.M. Yusuf, M. Sanyal, M. Sastry, Small 2 (2006) 135–141.
[17] P. Mukherjee, A. Ahmad, D. Mandal, S. Senapati, S.R. Sainkar, M.I. Khan, R. Parishcha, P.V. Ajaykumar, M. Alam, R. Kumar, M. Sastry, Nano Lett. 1 (2001) 515–519.
[18] R.Y. Parikh, S. Singh, B.L.V. Prasad, M.S. Patole, M. Sastry, Y.S. Shouche, ChemBioChem 9 (2008) 1415–1422.
[19] T. Klaus, R. Joerger, E. Olsson, C.G. Granqvist, Proc. Natl. Acad. Sci. USA 96 (1999) 13611–13614.
[20] M. Kowshik, A. Shriwas, K. Sharmin, W. Vogel, J. Urban, S.K. Kulkarni, K.M. Paknikar, Nanotechnology 14 (2003) 95–100.
[21] E.A. Mazzio, K.F.A. Soliman, J. Appl. Toxicol. 24 (2004) 99–106.
[22] Y. Komazaki, T. Inoue, S. Tanaka, Analyst 126 (2001) 587–593.
[23] O. Wolfbeis, A. Drkop, M. Wu, Z. Lin, Angew. Chem. Int. Ed. 41 (2002) 4495–4498.
[24] K.M. Wang, J. Li, X.H. Yang, F.L. Shen, X. Wang, Sens. Actuators B 65 (2000) 239–240.
[25] J. Jia, B. Wang, A. Wu, G. Cheng, Z. Li, S. Dong, Anal. Chem. 74 (2002) 2217–2223.
[26] S.J. Guo, E.K. Wang, Anal. Chim. Acta 598 (2007) 181–192.
[27] U.Y. Jeong, Y.N. Xia, Adv. Mater. 17 (2005) 102–106.
[28] Z.H. Lin, C.R.C. Wang, Mater. Chem. Phys. 92 (2005) 591–594.
[29] U. Jeong, T. Herricks, E. Shahar, Y.N. Xia, J. Am. Chem. Soc. 127 (2005) 1098–1099.
[30] L.B. Yang, G.Y. Chen, J. Wang, T.T. Wang, M.Q. Li, J.H. Liu, J. Mater. Chem. 19 (2009) 6849–6856.
[31] G.C. Xi, K. Xiong, Q.B. Zhao, R. Zhang, H.B. Zhang, Y.T. Qian, Cryst. Growth Des. 6 (2006) 577–582.
[32] V. Bansal, P. Poddar, A. Ahmad, M. Sastry, J. Am. Chem. Soc. 128 (2006) 11958–11963.
[33] S. Senapati, A. Ahmad, M.I. Khan, M. Sastry, R. Kumar, Small 1 (2005) 517–520.
[34] V. Bansal, D. Rautaray, A. Bharde, K. Ahire, A. Sanyal, A. Ahmad, M. Sastry, J. Mater. Chem. 15 (2005) 2583–2589.
[35] M. Guan, W. Liu, Y.L. Shao, H.Y. Huang, H.X. Zhang, Micropor. Mesopor. Mater. 123 (2009) 193–201.
[36] Y.Q. Xia, T.Y. Guo, H.L. Zhao, M.D. Song, B.H. Zhang, B.L. Zhang, J. Biomed. Mater. Res. A 90A (2009) 326–332.
[37] S. Elhadj, A.A. Chernov, J.J.D. Yoreo, Nanotechnology 19 (2008) 105304–105312.
[38] R.L. Penn, J.F. Banfield, Science 281 (1998) 969–971.
[39] B. Gates, Y.D. Yin, Y.N. Xia, J. Am. Chem. Soc. 122 (2000) 12582–12583.
[40] U.Y. Jeong, P.H.C. Camargo, Y.H. Lee, Y.N. Xia, J. Mater. Chem. 16 (2006) 3893–3897.
[41] B.H. Liu, Z.J. Liu, D.D. Chen, J.L. Kong, J.Q. Deng, Fresenius J. Anal. Chem. 367 (2000) 539–544.
[42] X.C. Tan, J.L. Zhang, S.W. Tan, D.D. Zhao, Z.W. Huang, Y. Mi, Z.Y. Huang, Electroanalysis 21 (2009) 1514–1520.
[43] S. Chakraborty, C.R. Raj, Biosens. Bioelectron. 24 (2009) 3264–3268.
[44] S.J. Guo, D. Wen, S.J. Dong, E.K. Wang, Talanta 77 (2009) 1510–1517.
[45] V.P. Yissar, E. Katz, J. Wasserman, I. Willner, J. Am. Chem. Soc. 125 (2003) 622–623.
[46] A.C. Patel, S. Li, J.M. Yuan, Y. Wei, Nano Lett. 6 (2006) 1042–1046.
[47] L. Yu, I.A. Banerjee, X. Gao, N. Nuraje, H. Matsui, Bioconjug. Chem. 16 (2005) 1484–1487.
[48] L. Meng, L.G. Yang, B. Zhou, C.X. Cai, Nanotechnology 20 (2009) 35502–35509.